A new class of third-order nonlinear optical materials: laser pulse-duration dependant saturable absorption and nonlinear refraction in platinum(II) diimine-dithiolate complexes†‡

Anna Pintus, *[a] Cristian Pilloni,[a] Gabriele Pippia, [a] Enrico Podda,[a,b] M. Carla Aragoni, [a] Vito Lippolis, [a] Panagiotis Aloukos,[c,d] Dionysios Potamianos,§[c,d] Nikolaos Chazapis,[c,d] Stelios Couris, *[c,d] George C. Anyfantis,[e] Alexandra M. Z. Slawin, [f] J. Derek Woollins [f,g] and Massimiliano Arca *[a]

The third-order nonlinear optical (NLO) properties of a series of platinum diimine-dithiolate complexes [Pt(N^N)(S^S)] were investigated by means of *Z*-scan measurements, revealing second hyperpolarizability values up to 10^{-29} esu, saturable absorption properties, and nonlinear refractive behaviour, which were rationalized also by means of DFT calculations.

Introduction

Within the wider and largely investigated class of 1,2-dithiolene metal complexes,[1,2] the past thirty years have witnessed a great deal of interest in platinum diimine-dithiolate heteroleptic complexes [Pt(N^N)(S^S)] due to their unique properties[3] that include solution luminescence,[4] long-lived excited state oxidation potentials,[5] and a solvatochromic absorption band in the visible region[6] whose energy can be fine-tuned by structural modifications.[7–10] This absorption band is assigned to the HOMO → LUMO electronic transition, featuring a mixed metal/ligand-to-ligand charge-transfer (MMLL'CT) character,[11] since the LUMO is centred on the diimine N^N and the HOMO on the S^S 1,2-dithiolate ligand and partly on the metal.[12] Potential applications based on these properties include light-driven hydrogen generation,[13,14] and use in devices such as dye-sensitized solar cells[15,16] and photodetectors.[17,18] These systems also find applications as nonlinear optical (NLO) materials.[19] In particular, the second-order NLO properties of these systems were studied both experimentally[20,21] and theoretically,[8,22–24] prompted by their lack of an inversion centre. On the other hand, third-order NLO properties impose no symmetry constraints, so that, due to many important applications in optoelectronics,[25] these properties were studied in the past for various homoleptic 1,2-dithiolene metal complexes.[26–33] Surprisingly, the third-order NLO properties of heteroleptic[34,35] 1,2-dithiolene coordination compounds, and in particular [Pt(N^N)(S^S)] complexes,[36] have instead been investigated only occasionally in the past. In particular, no studies were reported on saturable absorption (SA) and nonlinear refraction (NLR),[37] despite possible applications to optical limiting[38] and switching.[39]

Given the unique optical properties of [Pt(N^N)(S^S)] systems and the ongoing search for new NLO materials with third-order nonlinear absorption and refraction properties, the investigation of SA and NLR in platinum diimine-dithiolate complexes was undertaken, and their potential as a new class of third-order NLO materials was assessed. In particular, herein we report on the synthesis, characterization, and third-order NLO properties of a series of [Pt(N^N)(S^S)] complexes

[a]*Dipartimento di Scienze Chimiche e Geologiche, Università degli Studi di Cagliari, S. S. 554 Bivio per Sestu, 09042 Monserrato, CA, Italy. E-mail: apintus@unica.it, marca@unica.it*
[b]*Centro Servizi di Ateneo per la Ricerca (CeSAR), Università degli Studi di Cagliari, S.S. 554 bivio per Sestu, 09042 Monserrato, CA, Italy*
[c]*Institute of Chemical Engineering Sciences (ICE-HT), Foundation for Research and Technology-Hellas (FORTH), P.O. Box 1414, 26504 Patras, Greece. E-mail: couris@upatras.gr*
[d]*Department of Physics, University of Patras, 26504 Patras, Greece*
[e]*NanoPhos S.A., Science and Technology Park of Lavrio, 1st km of Lavrio – Athens Ave., PO Box 519, Lavrio 19500, Attica, Greece*
[f]*EaStCHEM School of Chemistry, University of St. Andrews, North Haugh, KY16 9ST St. Andrews, Fife, UK*
[g]*Department of Chemistry, Khalifa University, Abu Dhabi 127788, United Arab Emirates*

†Dedicated to the memory of Prof. G. C. Papavassiliou.

‡Electronic supplementary information (ESI) available: Synthetic, computational, and crystallographic details, electrochemical, spectroscopic and NLO data, DFT-optimised geometries and relative metric parameters, eigenvalues, and drawings of frontier molecular orbitals, TD-DFT data, Jablonski diagrams. CCDC 2249965 and 2249966. For ESI and crystallographic data in CIF or other electronic format see DOI: https://doi.org/10.1039/d3dt00931a

§Present address: Ludwig-Maximilians-Universität München, Am Coulombwall 1, 85748 Garching, Germany.

featuring 5,6-dihydro-1,4-dithiin-2,3-dithiolate ($dddt^{2-}$) or 6,7-dihydro-5*H*-1,4-dithiepin-2,3-dithiolate ($pddt^{2-}$) as S^S ligands, along with 1,10-phenanthroline (phen) or 2,2′-bipiridine (bipy) as N^N derivatives.

Experimental

Materials and methods

Solvents (reagent-grade) were purchased from Honeywell and dried by using standard techniques. DMSO-d_6 was purchased form Eurisotop and stored under molecular sieves prior to use. Reagents were purchased from Alfa Aesar, Acros Organics, Chempur, Fluorochem, and Merck, and used without further purification. 5,6-Dihydro-1,3-dithiol-1,4-dithiin-2-one,[40] 6,7-dihydro-5*H*-1,3-dithiol-1,4-dithiepin-2-one[41] and the diimine-dichlorido complexes $[Pt(N^N)Cl_2]$[42,43] (N^N = 2,2′-bipyridine, 1,10-phenanthroline, 4,4′-dimethyl-2,2′-bipyridine, and 4,4′-di-*tert*-butyl-2,2′-bipyridine) were prepared according to published procedures. Uncorrected melting points were determined in capillaries on a FALC mod. C (up to 290 °C) melting point apparatus. Elemental analyses were performed with a CHNS/O PE 2400 series II elemental analyzer (T = 925 °C). FT-IR spectra were recorded with a Thermo-Nicolet 5700 spectrometer at room temperature. KBr pellets with a KBr beam splitter and KBr windows (4000–400 cm^{-1}, resolution 4 cm^{-1}) were used. UV-Vis absorption spectra were recorded at 25 °C in a quartz cell of 10.00 mm optical path with a Thermo Evolution 300 (190–1100 nm) spectrophotometer. ^{1}H-NMR measurements were carried out in DMSO-d_6 at 25 °C, using a Bruker Avance III HD 600 MHz spectrometer operating at the frequency of 600 MHz. Chemical shifts are reported in ppm (δ) and are calibrated to the solvent residue. Cyclic voltammetry measurements (scan rate in the range 20–150 mV s^{-1}) were performed at room temperature in anhydrous DMSO in a Metrohm voltammetric cell, with a combined platinum working and counter-electrode and a standard Ag/AgCl reference electrode with a Metrohm Autolab PGSTAT 10 potentiostat (supporting electrolyte 0.10 M $TBAPF_6$). Reported data are referred to the reversible Fc^+/Fc couple.

X-ray diffraction measurements

X-ray single-crystal diffraction data for complex **1** were collected using a Rigaku Saturn724 diffractometer operating at T = 125 K and using Mo Kα radiation. The data were indexed and processed using CrystalClear.[44] X-ray single-crystal diffraction data for complex **5** were collected on a Bruker D8 Venture diffractometer equipped with a PHOTON II area detector operating at T = 298 K and using Mo Kα radiation. The data were indexed and processed using Bruker SAINT[45] and SADABS.[46] The structures were solved with the ShelXT 2018[47] solution program using dual-space methods and by using Olex2[7] 1.5 as the graphical interface. The models were refined with ShelXL 2018[48] using full matrix least squares minimisation on F^2. All non-hydrogen atoms were refined anisotropically. Hydrogen atom positions were calculated geometrically and refined using the riding model. CCDC 2249965 (complex **1**) and CCDC 2249966 (complex **5**) contain the supplementary crystallographic data for this paper.‡

Synthesis

General procedure for the synthesis of complexes 1–6. Platinum diimine-dithiolate complexes [Pt(N^N)(S^S)] **1–6** were synthesised according to the following general procedure: a fourfold excess of NaOEt or KOH in ethanol was added dropwise under a N_2 inert atmosphere to an ethanol solution of the desired 1,2-dithiolate proligand; an equimolar suspension of the appropriate $[Pt(N^N)Cl_2]$ complex in tetrahydrofurane was then added, and the reaction mixture was left under magnetic stirring for seven days. The dark precipitate was collected by filtration and washed with ethanol and water.

[Pt(bipy)(dddt)] (1). Prepared from 5,6-dihydro-1,3-dithiol-1,4-dithiin-2-one (0.077 g, 0.370 mmol) in 20 mL of ethanol, and $[Pt(bipy)Cl_2]$ (0.156 g, 0.370 mmol) in 15 mL of THF. Crystals suitable for X-ray diffraction were obtained by slow evaporation of an acetone solution of the complex. Yield 0.114 g (58%). Mp: >290 °C. FT-IR: $\tilde{\nu}$ = 3077 (vw), 2957 (vw), 2903 (vw), 1969 (vw), 1815(vw), 1604 (m), 1488 (w), 1469 (s), 1443 (m), 1427 (m), 1411 (vw), 1312 (w), 1277 (vw), 1261 (vw), 1164 (vw), 1153 (w), 1120 (w), 1105 (vw), 1068 (w), 1045 (vw), 981 (vw), 942 (vw), 881 (w), 867 (vw), 746 (vs), 716 (m), 463 (vw), 452 (vw), 411 cm^{-1} (w). UV-vis-NIR (DMSO): λ (ε) = 302 (23 000), 375 (2000), 615 nm (4400 M^{-1} cm^{-1}). Elemental analysis calcd (%) for $C_{14}H_{12}N_2PtS_4$: C 31.63, H 2.28, N 5.27. Found: C 31.22, H 2.04, N 5.11. HR-ESI(+)-MS (MeCN solution) m/z: 530.9532 (calcd 530.9531) for $[C_{14}H_{13}N_2PtS_4]^+$ $[M + H]^+$. ^{1}H-NMR (600 MHz, DMSO-d_6): δ = 8.98 (d, 2H), 8.63 (d, 2H), 8.35 (t, 2H), 7.73 (t, 2H), 2.97 ppm (s, 4H). CV (DMSO): $E_{1/2}$ *vs.* Fc^+/Fc (scan rate 100 mV s^{-1}) = −1.728, −0.177 V.

[Pt(bipy)(pddt)] (2). Prepared from 6,7-dihydro-5*H*-1,3-dithiol-1,4-dithiepin-2-one (0.0823 g, 0.370 mmol) in 20 mL of ethanol, and $[Pt(bipy)Cl_2]$ (0.165 g, 0.369 mmol) in 15 mL of THF. Yield 0.135 g (67%). Mp: >290 °C. FT-IR: $\tilde{\nu}$ = 3068 (w), 2901 (w), 2890 (w), 2865 (w), 1603 (m), 1488 (w), 1469 (s), 1445 (s), 1429 (w), 1401 (m), 1313 (w), 1273 (m), 1261 (w), 1244 (w), 1156 (w), 1123 (w), 1068 (w), 1045 (vw), 1032 (vw), 997 (vw), 895 (w), 874 (w), 858 (vw), 816 (vw), 795 (vw), 749 (vs), 716 (m), 665 (vw), 646 (vw), 583 (vw), 469 (w), 412 cm^{-1} (w). UV-vis-NIR (DMSO): λ (ε) = 298 (22 600), 325 (sh, 10 000), 580 nm (4100 M^{-1} cm^{-1}). Elemental analysis calcd (%) for $C_{15}H_{14}N_2PtS_4$: C 33.02, H 2.59, N 5.13. Found: C 33.40, H 2.29, N 5.05. HR-ESI(+)-MS (MeCN solution) m/z: 544.9692 (calcd 544.9688) for $[C_{15}H_{15}N_2PtS_4]^+$ $[M + H]^+$. ^{1}H-NMR (600 MHz, DMSO-d_6): δ = 8.97 (d, 2H), 8.63 (d, 2H), 8.34 (t, 2H), 7.75 (t, 2H), 2.58 (m, 4H), 2.32 ppm (m, 2H). CV (DMSO): $E_{1/2}$ *vs.* Fc^+/Fc (scan rate 100 mV s^{-1}) = −1.678, −0.112 V.

[Pt(phen)(dddt)] (3). Prepared from 5,6-dihydro-1,3-dithiol-1,4-dithiin-2-one (0.0427 g, 0.205 mmol) in 15 mL of ethanol, and $[Pt(phen)Cl_2]$ (0.0905 g, 0.203 mmol) in 15 mL of THF. Yield 0.085 g (75%). Mp: >290 °C. FT-IR: $\tilde{\nu}$ = 3044 (w), 2944 (vw), 2906 (w), 1630 (w), 1619 (w), 1598 (vw), 1578 (vw), 1513 (vw), 1492 (w), 1450 (w), 1430 (s), 1412 (m), 1385 (vw), 1344 (w), 1315 (w), 1292 (w), 1285 (w), 1258 (vw), 1221 (w), 1202 (w),

1172 (vw), 1141 (w), 1094 (w), 1059 (vw), 945 (vw), 919 (vw), 872 (w), 827 (s), 752 (vw), 725 (w), 706 (vs), 603 (vw), 505 (vw), 469 (vw), 414 cm^{-1} (vw). UV-vis-NIR (DMSO): λ (ε) = 366 (4100), 611 nm (4500 M^{-1} cm^{-1}). Elemental analysis calcd (%) for $C_{16}H_{12}N_2PtS_4$: C 34.59, H 2.18, N 5.04. Found: C 33.97, H 2.29, N 4.75. HR-ESI(+)-MS (MeCN solution) *m*/*z*: 544.9532 (calcd 554.9531) for $[C_{16}H_{13}N_2PtS_4]^+$ $[M + H]^+$. ^{1}H-NMR (600 MHz, DMSO-d_6): δ = 9.30 (d, 2H), 8.96 (d, 2H), 8.26 (s, 2H), 8.06 (t, 2H), 3.00 ppm (s, 4H). CV (DMSO): $E_{1/2}$ *vs.* Fc^+/Fc (scan rate 100 mV s^{-1}) = −1.676, −0.192 V.

[Pt(phen)(pddt)] (4). Prepared from 6,7-dihydro-5*H*-1,3-dithiol-1,4-dithiepin-2-one (0.0628 g, 0.282 mmol) in 20 mL of ethanol, and [Pt(phen)Cl_2] (0.124 g, 0.279 mmol) in 20 mL of THF. Yield 0.100 g (62%). Mp: >290 °C. FT-IR: $\tilde{\nu}$ = 3054 (w), 2943 (w), 2902 (m), 2820 (vw), 1631 (w), 1619 (w), 1579 (vw), 1514 (vw), 1494 (w), 1471 (m), 1431 (s), 1411 (m), 1343 (vw), 1300 (w), 1272 (m), 1239 (w), 1220 (w), 1203 (vw), 1177 (vw), 1145 (w), 1095 (w), 996 (w), 969 (w), 931 (w), 901 (w), 881 (m), 856 (w), 830 (vs), 761 (m), 725 (w), 705 (s), 504 cm^{-1} (w). UV-vis-NIR (DMSO): λ (ε) = 334 (6200), 588 nm (5600 M^{-1} cm^{-1}). Elemental analysis calcd (%) for $C_{17}H_{14}N_2PtS_4$: C 35.85, H 2.48, N 4.92. Found: C 35.46, H 2.47, N 4.71. HR-ESI(+)-MS (MeCN solution) *m*/*z*: 568.9690 (calcd 568.9688) for $[C_{17}H_{15}N_2PtS_4]^+$ $[M + H]^+$. ^{1}H-NMR (600 MHz, DMSO-d_6): δ = 9.30 (d, 2H), 8.96 (d, 2H), 8.25 (s, 2H), 8.09 (t, 2H), 2.62 (m, 4H), 2.60 ppm (m, 2H). CV (DMSO): $E_{1/2}$ *vs.* Fc^+/Fc (scan rate 100 mV s^{-1}) = −1.683, −0.072 V.

[Pt(Me$_2$bipy)(dddt)] (5). Prepared from 5,6-dihydro-1,3-dithiol-1,4-dithiin-2-one (0.0910 g, 0.437 mmol) in 20 mL of ethanol, and [Pt(Me$_2$bipy)Cl_2] (0.200 g, 0.444 mmol) in 20 mL of THF. Crystals suitable for X-ray diffraction were obtained by slow evaporation of a DMF solution of the complex. Yield 0.204 g (83%). Mp: >290 °C. FT-IR: $\tilde{\nu}$ = 3060 (vw), 3029 (vw), 2960 (vw), 2916 (w), 1621 (vs), 1489 (s), 1444 (m), 1429 (m), 1377 (w), 1304 (w), 1284 (w), 1262 (w), 1250 (w), 1221 (vw), 1166 (w), 1099 (m), 1040 (w), 1032 (w), 925 (vw), 882 (w), 870 (vw), 819 (vs), 513 (m), 481 (vw), 461 (vw), 412 cm^{-1} (w). UV-vis-NIR (DMSO): λ (ε) = 299 (24 700), 365 (2100), 593 nm (4200 M^{-1} cm^{-1}). Elemental analysis calcd (%) for $C_{16}H_{16}N_2PtS_4$: C 34.34, H 2.88, N 5.01. Found: C 33.84, H 2.91, N 4.95. HR-ESI (+)-MS (MeCN solution) *m*/*z*: 558.9841 (calcd 558.9844) for $[C_{16}H_{17}N_2PtS_4]^+$ $[M + H]^+$. ^{1}H-NMR (600 MHz, DMSO-d_6): δ = 8.77 (d, 2H), 8.49 (s, 2H), 7.56 (d, 2H), 2.96 (s, 4H), 2.45 ppm (s, 6H). CV (DMSO): $E_{1/2}$ *vs.* Fc^+/Fc (scan rate 100 mV s^{-1}) = −1.778, −0.182 V.

Pt(^{t}Bu$_2$bipy)(dddt) (6). Prepared from 5,6-dihydro-1,3-dithiol-1,4-dithiin-2-one (0.0575 g, 0.276 mmol) in 20 mL of ethanol, and [Pt(^{t}Bu$_2$bipy)Cl_2] (0.150 g, 0.281 mmol) in 15 mL of THF. Yield 0.126 g (71%). Mp: >290 °C. FT-IR: $\tilde{\nu}$ = 2954 (vs), 2909 (m), 2866 (m), 1616 (vs), 1541 (w), 1486 (s), 1463 (m), 1450 (m), 1417 (s), 1396 (w), 1365 (m), 1304 (vw), 1284 (w), 1265 (m), 1252 (m), 1203 (w), 1157 (w), 1130 (w), 1075 (vw), 1037 (vw), 1029 (vw), 976 (vw), 927 (w), 903 (w), 880 (m), 847 (vs), 775 (vw), 738 (w), 598 (s), 464 (vw), 424 cm^{-1} (w). UV-vis-NIR (DMSO): λ (ε) = 301 (27 200), 364 (2200), 595 nm (5200 M^{-1} cm^{-1}). Elemental analysis calcd (%) for $C_{22}H_{28}N_2PtS_4$: C 41.04, H 4.38, N 4.35. Found: C 40.55, H 3.99, N 4.21. HR-ESI (+)-MS (MeCN solution) *m*/*z*: 643.0799 (calcd 643.0783) for $[C_{22}H_{29}N_2PtS_4]^+$ $[M + H]^+$. ^{1}H-NMR (600 MHz, DMSO-d_6): δ = 8.82 (d, 2H), 8.60 (s, 2H), 7.74 (d, 2H), 2.96 (s, 4H), 1.42 ppm (s, 18H). CV (DMSO): $E_{1/2}$ *vs.* Fc^+/Fc (scan rate 100 mV s^{-1}) = −1.819, −0.178 V.

Nonlinear optical measurements

The third-order NLO properties of complexes **1–6** were determined by means of the *Z*-scan technique under 4 ns and 35 ps laser excitation conditions, employing, in both cases, the fundamental and SHG outputs, at 1064 and 532 nm respectively, from a 4 ns Q-switched and a 35 ps mode-locked Nd:YAG laser systems, both operating at a repetition rate 1–10 Hz. This technique was chosen as it allows for the simultaneous determination of both the magnitude and the sign of the nonlinear absorption (*i.e.*, the nonlinear absorption coefficient β) and refraction (*i.e.*, nonlinear refractive index parameter γ') of a sample from a single measurement. Since the details of the *Z*-scan technique have been described in detail elsewhere,[49,50] only a brief description will be presented here. According to the formalism of *Z*-scan, the normalized transmittance of a sample moving along the propagation direction of a focused laser beam (*e.g.*, *z*-axis), is measured simultaneously by two different experimental configurations, the so-called "open-aperture" (OA) and "closed-aperture" (CA) *Z*-scans. In the former measurement, the transmitted through the sample laser beam is totally collected by a large diameter lens and provides information about the sample's nonlinear absorption. Simultaneously, in the latter, the transmitted through the sample laser beam is measured after having passed through a narrow aperture positioned in the far field, providing information on the sample's nonlinear refraction. The OA *Z*-scan recording can present a transmission minimum or maximum, denoting reverse saturable absorption (RSA, corresponding to $\beta > 0$) or saturable absorption (SA, corresponding to $\beta < 0$), respectively. Correspondingly, the presence of a transmission valley–peak or peak–valley configuration in the CA *Z*-scan indicates self-focusing (corresponding to $\gamma' > 0$) or self-defocusing (corresponding to $\gamma' < 0$) behaviour. In the case where the nonlinear absorption of the sample is negligible, the nonlinear refractive index parameter γ' can be directly deduced for the CA *Z*-scan, while under non negligible nonlinear absorption, the nonlinear refractive index parameter γ' is deduced from the so-called "divided" *Z*-scan obtained from the division of the CA *Z*-scan trace by the corresponding OA one.

The nonlinear absorption coefficient β is calculated by fitting the experimental OA *Z*-scan curve with the following eqn (1):

$$T = \frac{1}{\sqrt{\pi}\left[\frac{\beta I_0 L_{\text{eff}}}{(1+z^2/z_0^2)}\right]} \int_{-\infty}^{+\infty} \ln\left[1 + \frac{\beta I_0 L_{\text{eff}}}{(1+z^2/z_0^2)} \exp(-t^2)\right] \mathrm{d}t \quad (1)$$

where $L_{\text{eff}} = |1 - \exp(\alpha_0 L)|\alpha_0$ is the effective sample thickness; α_0 is the absorption coefficient at the laser excitation wave-

length; L is the sample length; I_0 is the laser peak irradiance on the focal plane; z_0 is the Rayleigh length; and z is the position of the sample along the z-axis.

Accordingly, the nonlinear refractive index parameter γ' can be determined by fitting the corresponding "divided" Z-scan with eqn (2):

$$\gamma' = \frac{\lambda\alpha_0}{1-\mathrm{e}^{-\alpha_0 L}}\frac{\Delta T_{\mathrm{p-v}}}{0.812\pi I_0(1-S)^{0.25}} \quad (2)$$

where $\Delta T_{\mathrm{p-v}}$ is the total variation of the normalized transmittance of the sample measured by the divided Z-scan; $S = 1-\exp\left(\frac{-2{r_\mathrm{a}}^2}{{w_\mathrm{a}}^2}\right)$ is the aperture linear transmittance, with r_a and w_a being the aperture and beam radii respectively and α_0, L and I_0 as defined previously.

Then, from the determined NLO parameters, β and γ', the corresponding imaginary and real parts, respectively, of the third-order susceptibility $\chi^{(3)}$ can be obtained from the following relations:

$$\mathrm{Im}\chi^{(3)}(\mathrm{esu}) = \frac{10^{-7}c^2{n_0}^2}{96\pi^2\omega}\beta(\mathrm{cm\,W^{-1}}) \quad (3)$$

$$\mathrm{Re}\chi^{(3)}(\mathrm{esu}) = \frac{10^{-6}c{n_0}^2}{480\pi^2}\gamma'(\mathrm{cm^2\,W^{-1}}) \quad (4)$$

where c is the speed of light in cm $\mathrm{s^{-1}}$, ω is the excitation frequency in $\mathrm{s^{-1}}$, and n_0 is the linear refractive index.

Since the third-order susceptibility $\chi^{(3)}$ is a macroscopic quantity, depending on the concentration of the solute, often, the second hyperpolarizability γ is preferred, which is a molecular constant, describing the NLO response per molecule, therefore allowing for direct comparisons. The second hyperpolarizability γ can be obtained from the third-order susceptibility $\chi^{(3)}$ using the following relation:

$$\gamma = \frac{\chi^{(3)}}{\mathrm{N}L^4} \quad (5)$$

where N is the number of molecules $\mathrm{cm^{-3}}$ and $L = \frac{({n_0}^2+2)}{3}$ is the Lorenz–Lorentz local field correction factor.

The Z-scan measurements were performed on solutions at different concentrations of the studied complexes **1–6** in DMF placed in 1 mm thick quartz cells, by using different laser intensities. The absorption spectra of all samples were regularly checked during the experiments to ensure their photostability upon laser irradiation and their concentration as well. For the experiments, the laser beam was focused into the sample by means of a 20 cm focal length quartz planoconvex lens. The beam spot radius at the focal plane was measured with a charge-coupled device (CCD) and was found to be ~30 and ~18 μm at 1064 and 532 nm, respectively, for both ns and ps lasers. The laser beam energy was monitored by means of a calibrated joulemeter. From the fitting of the OA Z-scans the NLO absorption coefficient β of each solution was determined, while from the slopes of the curves showing the variation of the $\Delta T_{\mathrm{p-v}}$ parameter with the peak irradiance, the corresponding NLO refractive index parameter γ' was also obtained. The NLO response of the neat solvent (*i.e.*, DMF) measured separately for the same range of laser intensities was found negligible for all excitation conditions used (*i.e.*, 1064 and 532 nm, for both ns and ps laser pulses).

Computational details

The computational investigation on complexes **1–6** was carried out at the DFT level[51] by adopting the Gaussian 16[52] suite of programs. A preliminary validation of the computational setup was carried out by comparing selected optimised distances for complex **1** with the corresponding structural data. The mPW1PW,[53] PBE0,[54] and B3LYP[55] functionals were tested in combination with LANL08(f),[56] CRENBL,[57] and Stuttgart RSC 1997[58] basis sets (BSs) with Relativistic Effective Core Potentials (RECPs)[59,60] on the heavier platinum species, and by adopting def2-SVP,[61] cc-pVDZ[62,63] and 6-311++G**[64,65] BSs on the lighter elements (C, H, N, and S). Basis sets were obtained from Basis Set Exchange and Basis Set EMSL Library.[66] A comparison between selected structural data and the corresponding optimised metric parameters (Table S6‡) showed that very similar results (RMSE = 0.014–0.016 for mPW1PW/PBE0 functionals; 0.022–0.028 for B3LYP) were obtained when using the mPW1PW and PBE0 functionals, both with the LANL08(f) and CRENBL basis sets for the central metal ion. Eventually, the PBE0 functional[54] was adopted due to its reportedly best performance in evaluating electronic transition energies. Based on these considerations, calculations were extended to complexes **2–6** at the PBE0//cc-pVDZ/LANL08(f) level of theory. In the case of complex **1**, two different geometries were optimised, a symmetric one where the complex molecule was allowed to belong to an ideal C_s point group, and a second one where the symmetry at the terminal $-CH_2-CH_2-$ moiety of the 1,2-dithiolene $\mathrm{dddt^{2-}}$ ligand was removed, in analogy with the conformation observed in the X-ray crystal structure of the complex. The latter was found to be the more stable, while the symmetric geometry showed negative values in the harmonic frequency calculation. Hence, in complexes **3**, **5**, and **6** the $\mathrm{dddt^{2-}}$ ligand was arranged in the asymmetric conformation. Geometry optimizations in the singlet ground state (S_0 in Fig. 6 and S11‡) were performed starting from structural data, when available. Furthermore, the triplet states at the lowest energy (T_1 in Fig. 6 and Fig. S11‡) were optimised. Fine numerical integration grids were used and the nature of the minima of the optimised structures was verified by full harmonic frequency calculations. Geometries optimised in the gas phase (Tables S7, S10, S13, S16, S19, and S28‡) were found to be in good agreement with the corresponding structural data, bond lengths and angles differing by less than 0.03 Å and 1.0°, respectively. Solvation calculations were also carried out at the same level of theory (Tables S8, S9, S11, S12, S14, S15, S17, S18, S20–27, S29, and S30‡), by using the integral equation formalism of the polarizable continuous model within the self-consistent reaction field approach (IEF-PCM SCRF).[67] Negligible differences were observed between the geometries

optimised in the gas phase and in the different solvents (Tables S31–34‡), the bond lengths and angles differing by less than 0.02 Å and 3.0°, respectively, the most significant difference being the slight elongation of Pt–S and Pt–N bond lengths (by about 0.015 and 0.010 Å respectively) on passing from the gas phase to solvation calculations. A population analysis was carried out at the optimised geometries using the natural bonding orbital partitioning scheme.[68]

The total dipole moment μ, linear average polarizability α, total first static hyperpolarizability β, and static average second hyperpolarizability γ were calculated at the optimised geometries[69–73] (polar = (cubc,DCSHG) keyword) by using the relations listed below, and the results are grouped in Tables S42–S53:‡

$$\mu = \sqrt{{\mu_x}^2 + {\mu_y}^2 + {\mu_z}^2} \quad (6)$$

$$\alpha = \frac{\alpha_{xx} + \alpha_{yy} + \alpha_{zz}}{3} \quad (7)$$

$$\beta = \sqrt{\left(\beta_{xxx} + \beta_{xyy} + \beta_{xzz}\right)^2 + \left(\beta_{yyy} + \beta_{yxx} + \beta_{yzz}\right)^2 + \left(\beta_{zxx} + \beta_{zyy} + \beta_{zzz}\right)^2} \quad (8)$$

$$\gamma = \frac{1}{5}\left[\gamma_{xxxx} + \gamma_{yyyy} + \gamma_{zzzz} + 2\left(\gamma_{xxyy} + \gamma_{xxzz} + \gamma_{yyzz}\right)\right] \quad (9)$$

Singlet and triplet absorption transitions energies E, wavelengths λ, and oscillator strength values f were calculated at the TD-DFT level of theory (100 singlet states and 50 triplet states were taken into account). The programs GaussView 6.0.16,[74] Molden 6.6,[75] and Chemissian 4.67[76] were used to investigate the optimised structures and the isosurfaces of Kohn–Sham molecular orbitals.

Results and discussion

Complexes **1–4**[77,78] and **6**,[79] previously reported, and newly prepared complex **5** (Scheme 1) were synthesised by reacting the corresponding dichlorido precursors [Pt(N^N)Cl_2][40,41] with the appropriate 1,2-dithiolato ligand, obtained *in situ* through the deprotection of the corresponding proligand (Scheme S1‡).

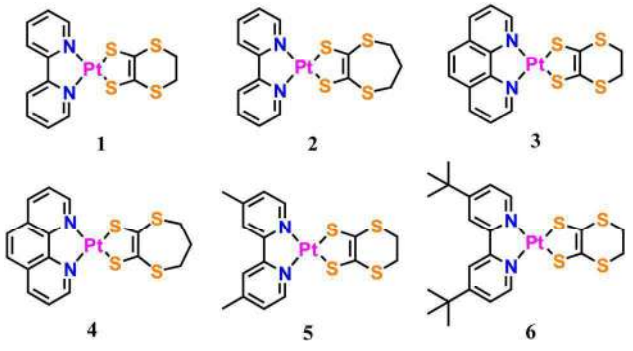

Scheme 1 Molecular structures of complexes **1–6**.

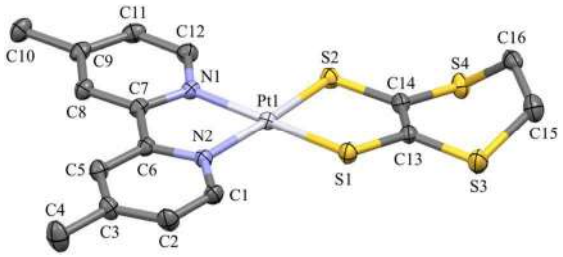

Fig. 1 Crystal structure of complex **5** with the atom labelling scheme adopted. Thermal ellipsoids are shown at the 30% probability level. Hydrogen atoms were omitted for clarity.

In the crystal structures of complexes **1** and **5** (Fig. 1 for **5**; Fig. S1 for **1**; Tables S1–S2‡), a slightly distorted square-planar coordination geometry is featured. Pt–S and Pt–N bond lengths [average 2.248 and 2.052 Å for **1**; 2.254 and 2.060 Å for **5**] are close to those found for complexes **2** (2.247 and 2.041 Å, respectively) and **6** (2.256 and 2.054 Å, respectively) and are in agreement with the relevant mean values observed for other structurally characterised [Pt(N^N)(S^S)] complexes[78–80] The C–C and C–S distances within the 1,2-dithiolato ligand [C–C: 1.337(8) and 1.345(6) Å for **1** and **5**, respectively; average C–S: 1.764 and 1.761 Å for **1** and **5**, respectively] confirm the ene-1,2-dithiolate form expected for the S^S ligand in diimine-dithiolate complexes.[1] The $dddt^{2-}$ ligand in complex **1** shows a disordered –S–CH_2–CH_2–S– moiety that was modelled over two sites with equal atomic occupancies (Fig. S1‡). In complex **5** the unsaturated portion of the $dddt^{2-}$ ligand is markedly folded with respect to the ene-1,2-dithiolate plane with an angle of 46.9° (Fig. 1), similarly to what previously reported for complex **6** (59.4°) and other complexes of this ligand.[79,81,82] In both crystal structures of complexes **1** and **5**, weak intermolecular interactions are responsible for the overall crystal packing. In the case of complex **5**, π–π interactions between the diimine and the 1,2-dithiolate metallacycle of a symmetry-related complex molecule (with an intercentroid distance of 3.74 Å) lead to the formation of weakly bonded dimers (Fig. S2‡), with Pt···Pt^i distances (3.77 Å; ^{i} = 1 − x, 1 − y, 1 − z) close to that previously encountered in [Pt(phen)(Et-dmet)] (3.80 Å; Et-$dmet^{2-}$ = *N*-ethyl-2-thioxoimidazoline-4,5-dithiolate).[8,83] The dimers interact along the *c*-axis through additional π–π stacking interactions between pyridyl moieties (intercentroid distance 3.64 Å).[84,85]

Cyclic voltammetry (CV) measurements in DMSO solution showed in all cases two monoelectronic redox processes at about −1.7/−1.8 and −0.1/−0.2 V *vs.* Fc^+/Fc (scan rate = 0.1 V s^{-1}, Table S3 and Fig. S3‡ for complex **5**). The i_{pc}/i_{pa} current ratios and the separation between anodic and cathodic peaks suggest in most cases quasi-reversible processes. The observed redox steps can be attributed to the reduction of the neutral complexes to their monoanionic forms and the oxidation to monocations, respectively. In agreement with previously drawn structure–property relationships,[8,86] a shift of the reduction towards more negative potentials is observed on passing from

complexes **1–4** to **5** and **6**, featuring alkyl-substituted diimine ligands. The oxidation occurs at more positive potentials for complexes **1** and **3**, bearing the $dddt^{2-}$ ligand, as compared to **2** and **4**, featuring the $pddt^{2-}$ ligand. It is worth mentioning that the CV studies previously reported for complexes **1–4** evidenced the same trend for the oxidation potential,[77] while no reduction was observed. On the other hand, the previous electrochemical characterization of complex **6** showed an additional reversible oxidation,[79] not detected under the experimental conditions adopted in this investigation. The aforementioned trends parallel those in the absorption wavelength of the typical solvatochromic band (Fig. 2 and Tables S4–S5‡), which falls at about 600 nm and undergoes a hypsochromic shift for complexes **1** and **3** as compared to the other complexes. The recorded values are in good agreement with those previously reported for complexes **1–4** and **6**.[77,79] The solvatochromic behaviour follows the trends previously observed for [Pt(N^N)(S^S)] complexes, both in terms of shape of the curves and accordance with the empirical scale proposed by Eisenberg (Fig. S4‡).[86]

The results of the CV and UV-Vis characterizations can be interpreted based on DFT calculations [PBE0//cc-pVDZ/LANL08(f); Tables S6–S38 and Fig. S5–S6‡] performed both in the gas phase and in different solvents (IEF-PCM SCRF solvation model).[67] QM calculations confirm the expected frontier molecular orbital (MO) composition, with the Kohn–Sham (KS) HOMO centred on the partially negatively charged 1,2-dithiolato ligand and the KS-LUMO mainly localised on the diimine, bearing a partial positive natural charge. The central metal ion contributes to both MOs (Fig. 3 for complex **5**; Tables S35–S36 and Fig. S6‡).

A stabilization of KS-HOMO is calculated on passing from complex **1** and **3** to **2** and **4**, thus accounting for the more positive oxidation potentials observed experimentally. On the other hand, alkyl-substituted compounds **5** and **6** exhibit higher KS-LUMO eigenvalues as compared to **1–4**, consistent with their more negative reduction potentials (Table S37‡). Time-dependent DFT (TD-DFT) calculations also confirm the assignment of the absorption transition in the visible region to the HOMO → LUMO monoelectronic excitation, and the trend in

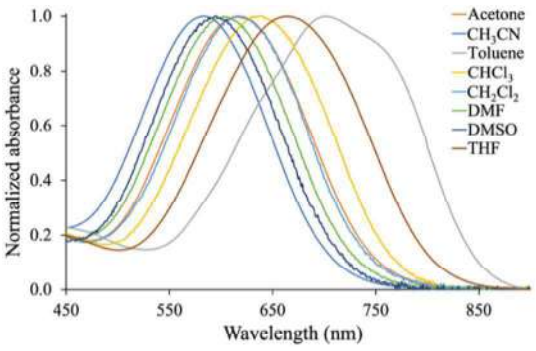

Fig. 2 Normalized absorption spectra in the visible region (450–900 nm) recorded for complex **6** in selected solvents.

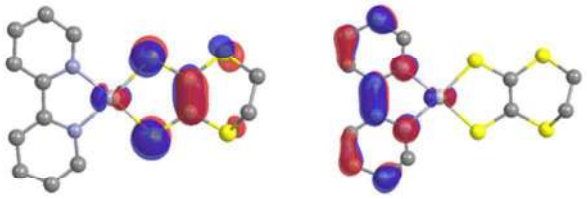

Fig. 3 KS-HOMO (left) and LUMO (right) isosurfaces calculated for complex **5** at the DFT level [PBE0//cc-PVDZ/LANL08(f)] in DMSO (IEF-PCM SCRF). Hydrogen atoms were omitted for clarity. Isovalue 0.05 |e|.

both the HOMO–LUMO energy gaps and the calculated absorption maxima closely reflect the experimental solvatochromic behaviour (Tables S38–S40‡).

The third-order nonlinear optical (NLO) response of complexes **1–6** was investigated by means of the *Z*-scan technique, using 4 ns and 35 ps laser pulses, both in the visible (532 nm) and infrared (1064 nm) regions, for different concentration solutions and at different laser intensities.

It is worth noting that, although some of the complexes herein have already been reported in the literature, an integrated analysis of their linear and nonlinear optical properties in terms of structure–property relationships as a coherent library of compounds has never been carried out.[77–79]

Complexes **1–6** exhibited negligible NLO response under 4 ns, 1064 nm excitation. On the contrary, the "open aperture" (OA) *Z*-scan measurements performed under 4 ns, 532 nm excitation showed a saturable absorption (SA) behaviour (Fig. 4).

Concerning the NLO refraction, all complexes, except **2**, exhibited negative sign NLO refraction (*i.e.*, self-defocusing) as suggested by the corresponding "divided" *Z*-scans, which exhibited a peak–valley transmission configuration (Fig. 4). Interestingly, the "divided" *Z*-scans of complex **2** feature instead a valley–peak configuration at lower laser intensities (up to 30 MW cm^{-2}), which changes to peak–valley at higher intensities (50–70 MW cm^{-2}), indicative of a self-defocusing behaviour (Fig. 5). This can be due to saturation effects and/or multiphoton absorption phenomena taking place at higher laser intensities, also reflected in the broadening of OA *Z*-scans (Fig. 5).

Under 35 ps, 532 nm excitation, all complexes showed negligible NLO absorption and a positive sign NLO refraction (Fig. S7‡), with second hyperpolarizability (γ) values significantly smaller compared to those determined from the ns measurements (Tables 1 and S41‡).

This difference must be expected, because under short pulse laser excitation the NLO response of molecular systems arises mainly from the instantaneous electronic response of the system, while under ns excitation it includes contributions from longer time scale phenomena, such as population redistribution among excited states [*e.g.*, intersystem crossing (ISC) between the first singlet excited state (S_1) and the lowest triplet state (T_1)], molecular orientation, or vibrational contributions, resulting in a larger NLO response often referred to as transient

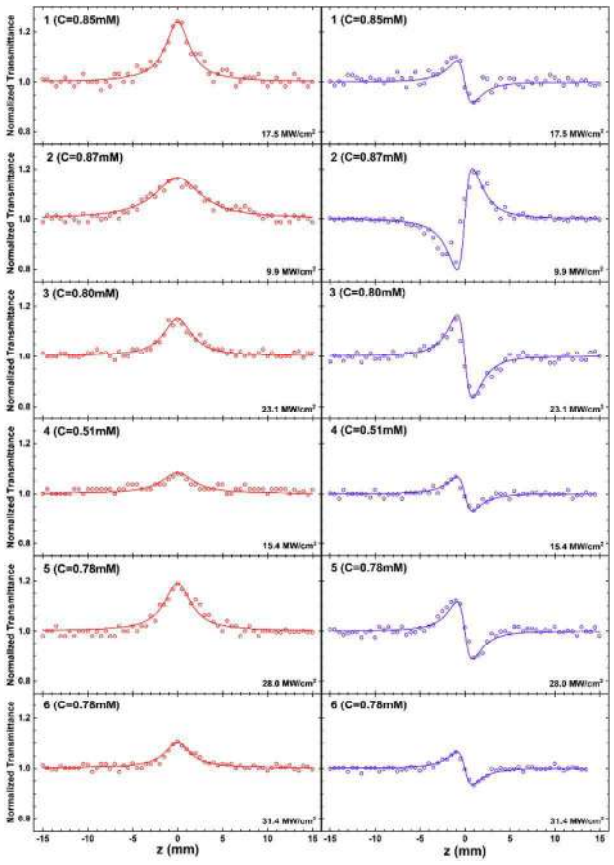

Fig. 4 "Open-aperture" (left) and "divided" (right) *Z*-scans of complexes **1–6** obtained under 4 ns, 532 nm laser excitation.

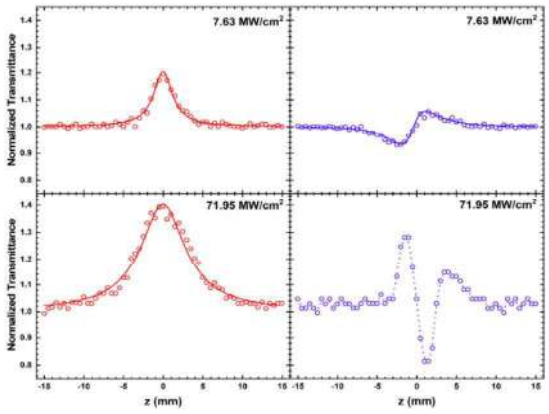

Fig. 5 "Open-aperture" (left) and "divided" (right) *Z*-scans of a 0.87 mM solution of complex **2** obtained under different laser intensities using 4 ns, 532 nm laser excitation.

NLO response.[29] The trend of γ values under ps excitation, showing similar values for all complexes, is mirrored by that calculated[69–73] at the DFT level in DMF, which accounts only for the electronic contribution of NLO processes (Tables S42–S53‡).

The variation of the ΔT_{p-v} parameter (determined from the "divided" *Z*-scans at different concentrations) with laser intensity shows a linear trend, suggesting a third order NLO response (Fig. S8‡). The OA *Z*-scans did not show any evidence of reverse saturable absorption (RSA), even for the highest laser intensities used, so that the occurrence of two- or multi-photon absorption processes can be excluded, as also confirmed by the lack of NLO response under 1064 nm excitation. The presence of SA can be thus rationalized in terms of efficient single photon absorption from the S_0 state.[26,32,34]

Table 1 Second hyperpolarizability γ ($\times 10^{-31}$ esu) values of complexes **1–6**, under 532 nm, 4 ns and 35 ps laser excitation

Complex	4 ns	35 ps
1	27 ± 1	1.24 ± 0.02
2	187 ± 30	1.70 ± 0.04
3	40 ± 3	2.5 ± 0.1
4	190 ± 25	3.36 ± 0.01
5	35 ± 2	2.0 ± 0.1
6	77 ± 10	2.9 ± 0.1

An overall evaluation of second hyperpolarizability values shows a good agreement with those determined for homoleptic or heteroleptic 1,2-dithiolene complexes under similar conditions, with γ values of the order of 10^{-30} and 10^{-31} esu for the ns and ps measurements, respectively (Table S54‡).[26,29,32,34,87–91] Complexes **2** and **4** were found to possess the largest second hyperpolarizabilities, particularly under ns laser excitation (1.87×10^{-29} and 1.90×10^{-29} esu for **2** and **4**, respectively, Table 1). Several factors might contribute to the larger NLO behaviour of complexes **2** and **4**. First, their absorption maxima in DMF (593 and 598 nm for **2** and **4**, respectively, Table S4‡) is the closest to the 532 nm wavelength used for the *Z*-scan measurements, resulting in the largest

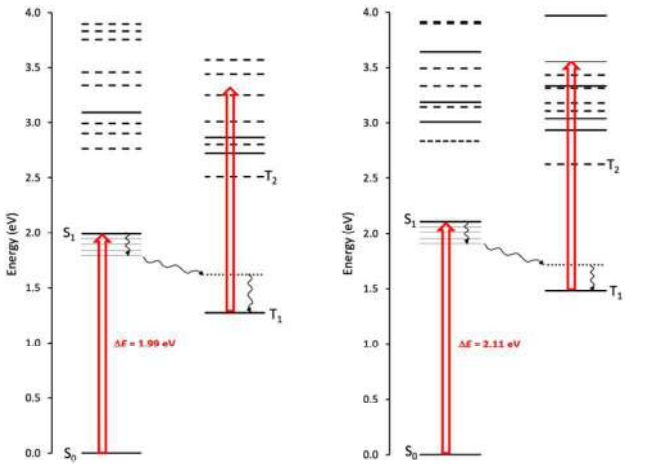

Fig. 6 Jablonski diagrams (0.0–4.0 eV) calculated for complexes **1** (left) and **2** (right) at TD-DFT level [PBE0//cc-pVDZ/LANL08(f)] in DMF (SCRF IEF-PCM). Excited states calculated for the $S_0 \rightarrow S_n$ and $T_1 \rightarrow T_n$ transitions with oscillator strength values $f < 0.05$ are represented as dashed lines. Red arrows represent energy gaps corresponding to the $S_0 \rightarrow S_1$ transition; wavy arrows correspond to the internal conversion of S_1, ISC between S_1 and the triplet state optimised at the same geometry (dotted line), and the internal conversion leading from the former to optimised T_1.

molar extinction coefficients at the excitation wavelength (ε_{532} = 2800 and 3800 M^{-1} cm^{-1} for complexes **2** and **4**, respectively, Fig. S9‡). Moreover, following a five-level model (Fig. S10‡),[92] the larger NLO absorption of complexes **2** and **4** under ns laser pulse might be attributed to a higher absorption contribution from excitation within the triplet states manifold. In fact, ISC between S_1 and T_1 can be induced by the spin–orbit coupling, typically enhanced in heavy atoms systems, such as Pt^{II} coordination compounds. The rate of ISC increases with the overlap between the vibrational wavefunctions of the initial and the final states, so that singlet and triplet quasi-degenerate states can be easily involved. After the ISC, a transition from T_1 to a higher triplet state T_n, resonant to the laser energy, can result in the SA effects.

A comparison of the Jablonski diagrams obtained from TD-DFT calculations shows in fact a denser pattern of excited triplet states in the region with T_n transitions of appropriate energy for complexes **2** and **4** compared, for example, to **1** (Fig. 6), where oscillator strengths f calculated for $T_1 \rightarrow T_n$ transitions in the relevant energy range are negligible ($f \leq 0.05$). In addition, in the case of **4**, a lower energy difference between S_1 and T_1 was computed (Fig. S11‡).

Conclusions

Different heteroleptic platinum diimine-dithiolate complexes were investigated in the present study, showing promising third-order NLO properties including saturable absorption and nonlinear refraction. Second hyperpolarizabilities values of up to 10^{-29} esu were observed under ns excitation, in the same order of magnitude as those observed for some of their homoleptic congeners. These results suggest that the NLO properties of [Pt(N^N)(S^S)] complexes are not limited to second-order effects, and that these systems also have potential as third-order NLO materials.

In particular, a NLR behaviour of negative sign is featured by the investigated complexes, with possible applications in ultrafast all-optical switching devices. Of particular interest are the results obtained for complex **2**, which shows a dependence of the sign of NLR on the intensity of incident radiation, thus suggesting applications in the field of tunable integrated light sources. Moreover, a dependence of the NLO properties on the combination of ligands in the different complexes was observed, and DFT calculations indicated that a combination of different electronic factors might be responsible for the different NLO behaviour within the library of compounds. These results suggest that the SA and NLR response in these materials could be modulated by fine structural modifications.

Future studies will be aimed at expanding this investigation to further complexes, based on the structure–property relationships elucidated herein.

Conflicts of interest

There are no conflicts to declare.

Acknowledgements

The authors acknowledge Fondazione di Sardegna (FdS Progetti Biennali di Ateneo, annualità 2018) for financial support. We acknowledge the CeSAR (Centro Servizi d'Ateneo per la Ricerca) of the University of Cagliari, Italy for the NMR, MS, and XRD analyses. MCA, MA, and AP kindly acknowledge CINECA for the computational resources on the GALILEO supercomputer accessed within the ISCRA project BIFLuoex. PA, DP, NC, and SC acknowledge Konstantinos Minotakis for helping in the NLO experiments.

References

1 E. I. Stiefel, *Dithiolene chemistry: Synthesis, properties, and applications*, Wiley, Hoboken, 2003.
2 M. Arca, M. C. Aragoni and A. Pintus, in *Handbook of Chalcogen Chemistry*, ed. F. A. Devillanova and W.-W. du Mont, RSC Publishing, Cambridge, 2013, pp. 127–179.
3 S. D. Cummings and R. Eisenberg, *Inorg. Chem.*, 1995, **34**, 2007–2014.
4 J. A. Zuleta, J. M. Bevilacqua and R. Eisenberg, *Coord. Chem. Rev.*, 1991, **111**, 237–248.
5 J. A. Zuleta, J. M. Bevilacqua, R. Eisenberg and J. M. Rehm, *Inorg. Chem.*, 1992, **31**, 1332–1337.
6 M. Hissler, J. E. McGarrah, W. B. Connick, D. K. Geiger, S. D. Cummings and R. Eisenberg, *Coord. Chem. Rev.*, 2000, **208**, 115–137.
7 J. A. Weinstein, M. T. Tierney, E. S. Davies, K. Base, A. A. Robeiro and M. W. Grinstaff, *Inorg. Chem.*, 2006, **45**, 4544–4555.
8 A. Pintus, M. C. Aragoni, N. Bellec, F. A. Devillanova, D. Lorcy, F. Isaia, V. Lippolis, R. A. M. Randall, T. Roisnel, A. M. Z. Slawin, J. D. Woollins and M. Arca, *Eur. J. Inorg. Chem.*, 2012, 3577–3594.
9 A. Pintus, M. C. Aragoni, S. J. Coles, S. L. Coles, F. Isaia, V. Lippolis, A. D. Musteti, F. Teixidor, C. Viñas and M. Arca, *Dalton Trans.*, 2014, **43**, 13649–13660.
10 A. Pintus, M. C. Aragoni, F. Isaia, V. Lippolis, D. Lorcy, A. M. Z. Slawin, J. D. Woollins and M. Arca, *Eur. J. Inorg. Chem.*, 2015, 5163–5170.
11 C. Makedonas, C. A. Mitsopoulou, F. J. Lahoz and A. I. Balana, *Inorg. Chem.*, 2003, **42**, 8853–8865.
12 C. A. Mitsopoulou, *Coord. Chem. Rev.*, 2010, **254**, 1448–1456.
13 G. Li, M. F. Mark, H. Lv, D. W. McCamant and R. Eisenberg, *J. Am. Chem. Soc.*, 2018, **140**, 2575–2586.
14 J. Zhang, P. Du, J. Schneider, P. Jarosz and R. Eisenberg, *J. Am. Chem. Soc.*, 2007, **129**, 7726–7727.
15 E. A. M. Geary, L. J. Yellowlees, L. A. Jack, I. D. H. Oswald, S. Parsons, N. Hirata, J. R. Durrant and N. Robertson, *Inorg. Chem.*, 2005, **44**, 242–250.
16 A. Islam, H. Sugihara, K. Hara, L. P. Singh, R. Katoh, M. Yanagida, Y. Takahashi, S. Murata, H. Arakawa and G. Fujihashi, *Inorg. Chem.*, 2001, **40**, 5371–5380.

17 C. Browning, J. M. Hudson, E. W. Reinheimer, F. L. Kuo, R. N. McDougald, H. Rabaâ, H. Pan, J. Bacsa, X. Wang, K. R. Dunbar, N. D. Shepherd and M. A. Omary, *J. Am. Chem. Soc.*, 2014, **136**, 16185–16200.

18 M. C. Aragoni, M. Arca, M. Binda, C. Caltagirone, V. Lippolis, D. Natali, E. Podda, M. Sampietro and A. Pintus, *Dalton Trans.*, 2021, **50**, 7527–7531.

19 R. W. Boyd, *Nonlinear optics*, Academic press, 2020.

20 S. D. Cummings, L. T. Cheng and R. Eisenberg, *Chem. Mater.*, 1997, **9**, 440–450.

21 K. Base, M. T. Tierney, A. Fort, J. Muller and M. W. Grinstaff, *Inorg. Chem.*, 1999, **38**, 287–289.

22 M. Y. Zhang, N. N. Ma, S. L. Sun, X. X. Sun, Y. Q. Qiu and B. Chen, *J. Organomet. Chem.*, 2012, **718**, 1–7.

23 C. Makedonas and C. A. Mitsopoulou, *Inorg. Chim. Acta*, 2007, **360**, 3997–4009.

24 S. Samiee and P. Hossienpour, *New J. Chem.*, 2019, **43**, 12865–12873.

25 J. V. Moloney, *Nonlinear optical materials*, Springer, New York, 1998.

26 P. Aloukos, G. Chatzikyriakos, I. Papagiannouli, N. Liaros and S. Couris, *Chem. Phys. Lett.*, 2010, **495**, 245–250.

27 M. C. Aragoni, M. Arca, T. Cassano, C. Denotti, F. A. Devillanova, R. Frau, F. Isaia, F. Lelj, V. Lippolis, L. Nitti, P. Romaniello, R. Tommasi and G. Verani, *Eur. J. Inorg. Chem.*, 2003, **2003**, 1939–1947.

28 T. Cassano, R. Tommasi, M. Arca and F. A. Devillanova, *J. Phys.: Condens. Matter*, 2006, **18**, 5279–5290.

29 G. Soras, N. Psaroudakis, G. A. Mousdis, M. J. Manos, A. J. Tasiopoulos, P. Aloukos, S. Couris, P. Labéguerie, J. Lipinski, A. Avramopoulos and M. G. Papadopoulos, *Chem. Phys.*, 2010, **372**, 33–45.

30 W. F. Guo, X. B. Sun, J. Sun, X. Q. Wang, G. H. Zhang, Q. Ren and D. Xu, *Chem. Phys. Lett.*, 2007, **435**, 65–68.

31 M. C. Aragoni, M. Arca, T. Cassano, C. Denotti, F. A. Devillanova, F. Isaia, V. Lippolis, D. Natali, L. Nitti, M. Sampietro, R. Tommasi and G. Verani, *Inorg. Chem. Commun.*, 2002, **5**, 869–872.

32 G. Chatzikyriakos, I. Papagiannouli, S. Couris, G. C. Anyfantis and G. C. Papavassiliou, *Chem. Phys. Lett.*, 2011, **513**, 229–235.

33 C. S. Winter, S. N. Oliver, R. J. Manning, J. D. Rush and C. Hill, *J. Mater. Chem.*, 1992, **2**, 443–448.

34 P. Aloukos, S. Couris, J. B. Koutselas, G. C. Anyfantis and G. C. Papavassiliou, *Chem. Phys. Lett.*, 2006, **428**, 109–113.

35 Z. Sun, M. Tong, H. Zeng, L. Ding, Z. Wang, Z. Xu, J. Dai and G. Bian, *Chem. Phys. Lett.*, 2001, **342**, 323–327.

36 J. Si, Q. Yang, Y. Wang, P. Ye, S. Wang, J. Qin and D. Liu, *Opt. Commun.*, 1996, **132**, 311–315.

37 A. Miller, in *Fabrication, properties and applications of low-dimensional semiconductors*, Springer, Dordrecht, 1995, pp. 383–413.

38 L. W. Tutt and T. F. Boggess, *Prog. Quantum Electron.*, 1993, **17**, 299–338.

39 M. Y. Kariduraganavar, R. V. Doddamani, B. Waddar and S. R. Parne, in *Nonlinear Optics – From Solitons to Similaritons*, ed. B. İlkay and A. Nalan, IntechOpen, London, 2021, p. 187.

40 J. Larsen and C. Lenoir, *Synthesis*, 1989, **1989**, 134.

41 K. Hartke, T. Kissel, J. Quante and R. Matusch, *Chem. Ber.*, 1980, **113**, 1898–1906.

42 G. T. Morgan and F. H. Burstall, *J. Chem. Soc.*, 1934, 965–971.

43 J. V. Rund, *Inorg. Chem.*, 1974, **13**, 738–740.

44 *Rigaku Crystal Clear-SM Expert, Software For Data Collection and Processing*, Rigaku Corporation, Tokyo (Japan), 2005.

45 *SAINT version 8.37 A*, Bruker AXS Inc., Wisconsin (USA), 2013.

46 *SADABS Version 2016/2*, Bruker AXS Inc., Wisconsin (USA), 2016.

47 G. M. Sheldrick, *SHELXT, Program for Crystal Structure Solution*, University of Göttingen, Göttingen (Germany), 2018.

48 G. M. Sheldrick, *SHELXL-2018/3 software package*, University of Göttingen, Göttingen (Germany), 2018.

49 M. Sheik-Bahae, E. W. Van Stryland and A. A. Said, *Opt. Lett.*, 1989, **14**, 955–957.

50 S. Couris, E. Koudoumas, A. A. Ruthf and S. Leacht, *J. Phys. B: At., Mol. Opt. Phys.*, 1995, **28**, 4537–4554.

51 W. Koch and M. C. Holthausen, *A chemist's guide to density functional theory*, Wiley-VCH, New York, 2001.

52 M. J. Frisch, G. W. Trucks, H. B. Schlegel, G. E. Scuseria, M. A. Robb, J. R. Cheeseman, G. Scalmani, V. Barone, G. A. Petersson, H. Nakatsuji, X. Li, M. Caricato, A. V. Marenich, J. Bloino, B. G. Janesko, R. Gomperts, B. Mennucci, H. P. Hratchian, J. V. Ortiz, A. F. Izmaylov, J. L. Sonnenberg, D. Williams-Young, F. Ding, F. Lipparini, F. Egidi, J. Goings, B. Peng, A. Petrone, T. Henderson, D. Ranasinghe, V. G. Zakrzewski, J. Gao, N. Rega, G. Zheng, W. Liang, M. Hada, M. Ehara, K. Toyota, R. Fukuda, J. Hasegawa, M. Ishida, T. Nakajima, Y. Honda, O. Kitao, H. Nakai, T. Vreven, K. Throssell, J. A. Montgomery, J. E. Peralta, F. Ogliaro, M. J. Bearpark, J. J. Heyd, E. N. Brothers, K. N. Kudin, V. N. Staroverov, T. A. Keith, R. Kobayashi, J. Normand, K. Raghavachari, A. P. Rendell, J. C. Burant, S. S. Iyengar, J. Tomasi, M. Cossi, J. M. Millam, M. Klene, C. Adamo, R. Cammi, J. W. Ochterski, R. L. Martin, K. Morokuma, O. Farkas, J. B. Foresman and D. J. Fox, *Gaussian 16 Rev. B. 01*, Wallingford, CT, 2016.

53 C. Adamo and V. Barone, *J. Chem. Phys.*, 1998, **108**, 664–675.

54 C. Adamo and V. Barone, *J. Chem. Phys.*, 1999, **110**, 6158–6170.

55 A. D. Beck, *J. Chem. Phys.*, 1993, **98**, 5646–5648.

56 L. E. Roy, P. J. Hay and R. L. Martin, *J. Chem. Theory Comput.*, 2008, **4**, 1029–1031.

57 R. B. Ross, J. M. Powers, T. Atashroo, W. C. Ermler, L. A. LaJohn and P. A. Christiansen, *J. Chem. Phys.*, 1998, **93**, 6654.

58 D. Andrae, U. Häußermann, M. Dolg, H. Stoll and H. Preuß, *Theor. Chim. Acta*, 1990, **77**, 123–141.

59 T. H. Dunning and P. J. Hay, in *Methods of Electronic Structure Theory*, ed. H. F. Schaefer, Plenum Press, New York, 1977, vol. 2, p. 1.

60 J. V. Ortiz, P. J. Hay and R. L. Martin, *J. Am. Chem. Soc.*, 1992, **114**, 2736–2737.

61 F. Weigend and R. Ahlrichs, *Phys. Chem. Chem. Phys.*, 2005, **7**, 3297–3305.

62 T. H. Dunning, *J. Chem. Phys.*, 1998, **90**, 1007–1023.

63 D. E. Woon and T. H. Dunning, *J. Chem. Phys.*, 1998, **98**, 1358–1371.

64 G. W. Spitznagel, T. Clark, P. von Ragué Schleyer and W. J. Hehre, *J. Comput. Chem.*, 1987, **8**, 1109–1116.

65 T. Clark, J. Chandrasekhar, G. W. Spitznagel and P. V. R. Schleyer, *J. Comput. Chem.*, 1983, **4**, 294–301.

66 K. L. Schuchardt, B. T. Didier, T. Elsethagen, L. Sun, V. Gurumoorthi, J. Chase, J. Li and T. L. Windus, *J. Chem. Inf. Model.*, 2007, **47**, 1045–1052.

67 J. Tomasi, B. Mennucci and R. Cammi, *Chem. Rev.*, 2005, **105**, 2999–3093.

68 A. E. Reed, R. B. Weinstock and F. Weinhold, *J. Chem. Phys.*, 1985, **83**, 735–746.

69 D. A. Kleinman, *Phys. Rev.*, 1962, **126**, 1977–1979.

70 H. A. Kurtz and D. S. Dudis, *Rev. Comput. Chem.*, 1998, 241–279.

71 G. Maroulis and A. Haskopoulos, *Comput. Theor. Chem.*, 2012, **988**, 34–41.

72 B. Baseia, F. A. P. Osório, L. F. Lima and C. Valverde, *Crystals*, 2017, **7**, 158.

73 S. Muhammad, *J. Mol. Graphics Modell.*, 2022, **114**, 108209.

74 R. Dennington, T. A. Keith and J. M. Millam, *GaussView, version 6.0. 16*, Semichem Inc., Shawnee Mission KS, 2016.

75 G. Schaftenaar and J. H. Noordik, *J. Comput.-Aided Mol. Des.*, 2000, **14**, 123–134.

76 L. V. Skripnikov, *Chemissian Version 4.53, Visualization Computer Program*, 2017.

77 T. M. Yao, J. L. Zuo and X. Z. You, *Transition Met. Chem.*, 1994, **19**, 614–618.

78 J. L. Zuo, R. G. Xiong, X. Z. You and X. Y. Huang, *Inorg. Chim. Acta*, 1995, **237**, 177–180.

79 F. Camerel, G. Albert, F. Barrière, C. Lagrost, M. Fourmigué and O. Jeannin, *Chem. – Eur. J.*, 2019, **25**, 5719–5732.

80 2.26(2) and 2.04(2) Å, respectively; calculated on 29 entries found in the Cambridge Structural Database (CSD) for [Pt (N^N)(S^S)] complexes (N^N = heterocyclic diimine; S^S = aromatic ene-1,2-dithiolate non embedded in aromatic ring), CCDC refcodes: BANDID, DURHIJ, DURHOP, EGIXUN, FEVYEL, GEMWOM, GEMWUS, GETJUK, LEXZIX, NISHOP, OJIWOT, OJIXAG, OJIXEK, OJIXIO, QODVEN, RESLAE, TEXHUA, TEXJAI, TEXJIQ, TICZUB, VECNOI, VECNUO, VECPAW, VECPEA, VECPIE, XIXFUG, XIXGAN, YIMZOK, and ZOXGOI.

81 G. C. Anyfantis, G. C. Papavassiliou, N. Assimomytis, A. Terzis, V. Psycharis, C. P. Raptopoulou, P. Kyritsis, V. Thoma and I. B. Koutselas, *Solid State Sci.*, 2008, **10**, 1729–1733.

82 J. H. Welch, R. D. Bereman and P. Singh, *Inorg. Chim. Acta*, 1989, **163**, 93–98.

83 M. C. Aragoni, M. Arca, F. A. Devillanova, F. Isaia, V. Lippolis, A. Mancini, L. Pala, A. M. Z. Slawin and J. D. Woollins, *Inorg. Chem.*, 2005, **44**, 9610–9612.

84 T. Dahl, D. Kozma, M. Ács, J. Weidlein, H. Schnöckel, G. B. Paulsen, R. I. Nielsen, C. E. Olsen, C. Pedersen and C. E. Stidsen, *Acta Chem. Scand.*, 1994, **48**, 95–106.

85 A. Moghimi, R. Alizadeh, H. Aghabozorg, A. Shockravi, M. C. Aragoni, F. Demartin, F. Isaia, V. Lippolis, A. Harrison, A. Shokrollahi and M. Shamsipur, *J. Mol. Struct.*, 2005, **750**, 166–173.

86 S. D. Cummings and R. Eisenberg, *J. Am. Chem. Soc.*, 1996, **118**, 1949–1960.

87 X. Q. Wang, Q. Ren, F. J. Zhang, W. F. Guo, X. B. Sun, J. Sun, H. L. Yang, G. H. Zhang, X. Q. Hou and D. Xu, *Mater. Res. Bull.*, 2008, **43**, 2342–2353.

88 J.-L. Zuo, T.-M. Yao, F. You, X.-Z. You, H.-K. Funb and B.-C. Yipb, *J. Mater. Chem.*, 1996, **6**, 1633–1637.

89 J. Dai, G. Q. Bian, X. Wang, Q. F. Xu, M. Y. Zhou, M. Munakata, M. Maekawa, M. H. Tong, Z. R. Sun and H. P. Zeng, *J. Am. Chem. Soc.*, 2000, **122**, 11007–11008.

90 G. C. Anyfantis, G. C. Papavassiliou, P. Aloukos, S. Couris, Y. F. Weng, H. Yoshino and K. Murata, *Z. Naturforsch., B: J. Chem. Sci.*, 2007, **62**, 200–204.

91 P. Aloukos, I. Papagiannouli, N. Liaros and S. Couris, in *International Conference on Transparent Optical Networks*, IEEE Computer Society, 2014.

92 B. J. Thompson, *Handbook of nonlinear optics*, Marcel Dekker, Inc., New York, 1996.